Structure of the γ–ε complex of ATP synthase

Andrew J. W. Rodgers and Matthew C. J. Wilce

Crystallography Centre and Department of Pharmacology, University of Western Australia and Western Australian Institute for Medical Research, Nedlands Western Australia 6907, Australia.

ATP synthases (F_1F_o-ATPases) use energy released by the movement of protons down a transmembrane electrochemical gradient to drive the synthesis of ATP, the universal biological energy currency. Proton flow through F_o drives rotation of a ring of c-subunits and a complex of the γ and ε-subunits, causing cyclical conformational changes in F_1 that are required for catalysis. The crystal structure of a large portion of F_1 has been resolved. However, the structure of the central portion of the enzyme, through which conformational changes in F_o are communicated to F_1, has until now remained elusive. Here we report the crystal structure of a complex of the ε-subunit and the central domain of the γ-subunit refined at 2.1 Å resolution. The structure reveals how rotation of these subunits causes large conformational changes in F_1, and thereby provides new insights into energy coupling between F_o and F_1.

ATP synthases (F_1F_o-ATPases) are highly conserved enzyme complexes located in inner bacterial and mitochondrial membranes, and chloroplast thylakoid membranes. Their primary role is to harness energy supplied by a proton gradient to synthesize ATP, although in some bacteria the enzyme can also function as an ATP-driven proton pump[1]. The complex consists of two major portions. In *Escherichia coli*, which possesses the simplest version of the enzyme, the water soluble portion F_1 has subunit stoichiometry $\alpha_3\beta_3\gamma\delta\varepsilon$ (ref. 1). The membrane-bound portion F_o, which functions as a proton pore, consists of one a-subunit, two b-subunits, and a ring of 10–12 c-subunits[2]. Proton flow at the interface of the a-subunit and the c-subunit ring is thought to drive rotation of the ring, along with the γ and ε-subunits, causing cyclical conformational changes in the catalytic sites in F_1 in accordance with the 'binding change' mechanism of ATP synthesis[3]. ATP driven rotation of the γ-subunit and the ε-subunit within F_1 has been observed experimentally[4–8]. A second connection between F_o and F_1, consisting of the two b-subunits and the δ-subunit, is thought to immobilize the $\alpha_3\beta_3$ hexamer and the a-subunit relative to γ–ε–c during catalysis.

Crystal structures of large portions of F_1 purified from bovine mitochondria (MF_1)[9] and rat liver mitochondria[10] show that the three α-subunits and three β-subunits are arranged alternately around a coiled pair of helices formed by the N- and C-termini of the γ-subunit. An incomplete structure of the central domain of the γ-subunit from *E. coli* has also recently been published[11]. In addition, while the structure of the isolated ε-subunit has been determined[12,13], the conformation of the bound protein is yet to be established. *In vitro*, γ and ε form a high affinity complex that has been shown to closely mimic that which forms between the two subunits in the F_1 holoenzyme[14]. Here we report the crystal structure refined at 2.1 Å resolution of a complex of the ε-subunit and the central domain of the γ-subunit (γ′; residues 11–258) from *E. coli*. We propose an arrangement by which this complex is likely to interact with the c-subunits and the $\alpha_3\beta_3$ hexamer, and suggest a model by which rotation of the γ–ε complex could bring about the large conformational changes in the catalytic sites required for ATP synthesis.

Overview of the γ′–ε structure

The structure of the ε-subunit within the γ′–ε complex consists of a 10-stranded β-sandwich at the N-terminus and two α-helices at the C-terminus (ε-α1, residues 88–103; ε-α2, residues115–138; Fig. 1*a*). The β-sandwich of ε within the complex is virtually identical to the uncomplexed form[13] (root mean square (r.m.s.) deviation of 0.658 Å for Cα atoms in residues 2–82). The C-terminal helices of ε, however, adopt dramatically different positions relative to the β-sandwich (see below). Within the γ′–ε complex, the β-sandwich of ε abuts a long pair of α-helices of γ consisting of N-terminal residues 12–56 (γ-α1) and C-terminal residues

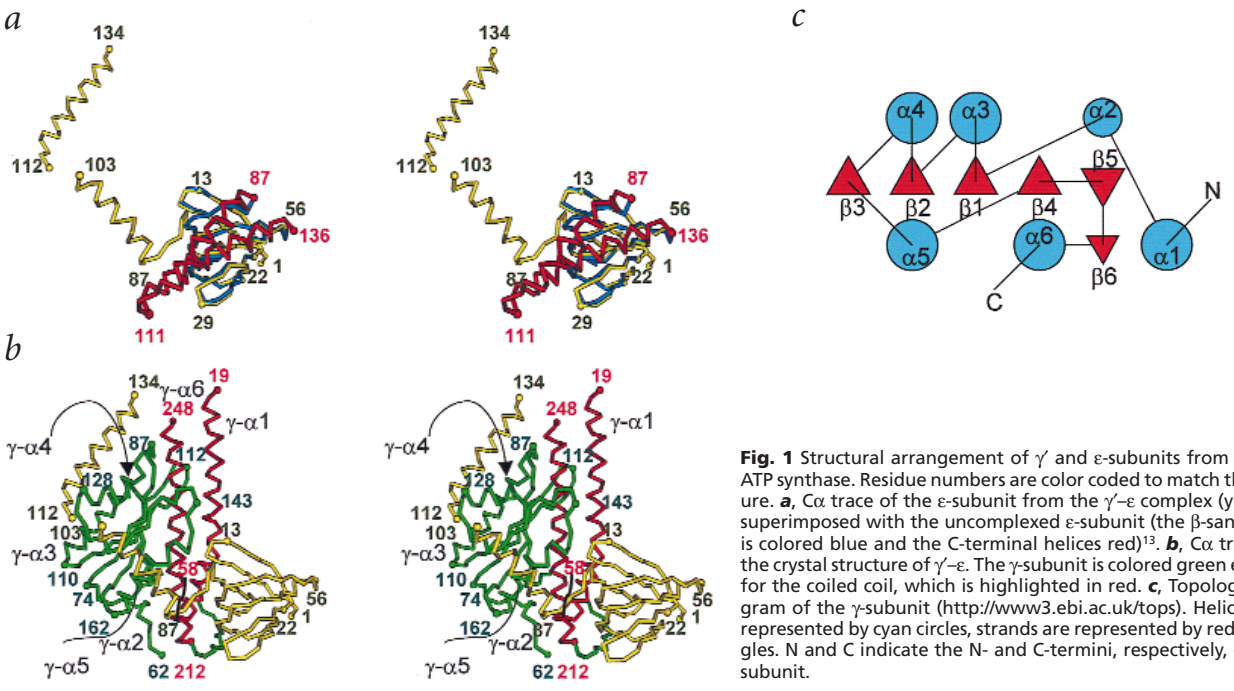

Fig. 1 Structural arrangement of γ′ and ε-subunits from *E. coli* ATP synthase. Residue numbers are color coded to match the figure. ***a***, Cα trace of the ε-subunit from the γ′–ε complex (yellow) superimposed with the uncomplexed ε-subunit (the β-sandwich is colored blue and the C-terminal helices red)[13]. ***b***, Cα trace of the crystal structure of γ′–ε. The γ-subunit is colored green except for the coiled coil, which is highlighted in red. ***c***, Topology diagram of the γ-subunit (http://www3.ebi.ac.uk/tops). Helices are represented by cyan circles, strands are represented by red triangles. N and C indicate the N- and C-termini, respectively, of the subunit.

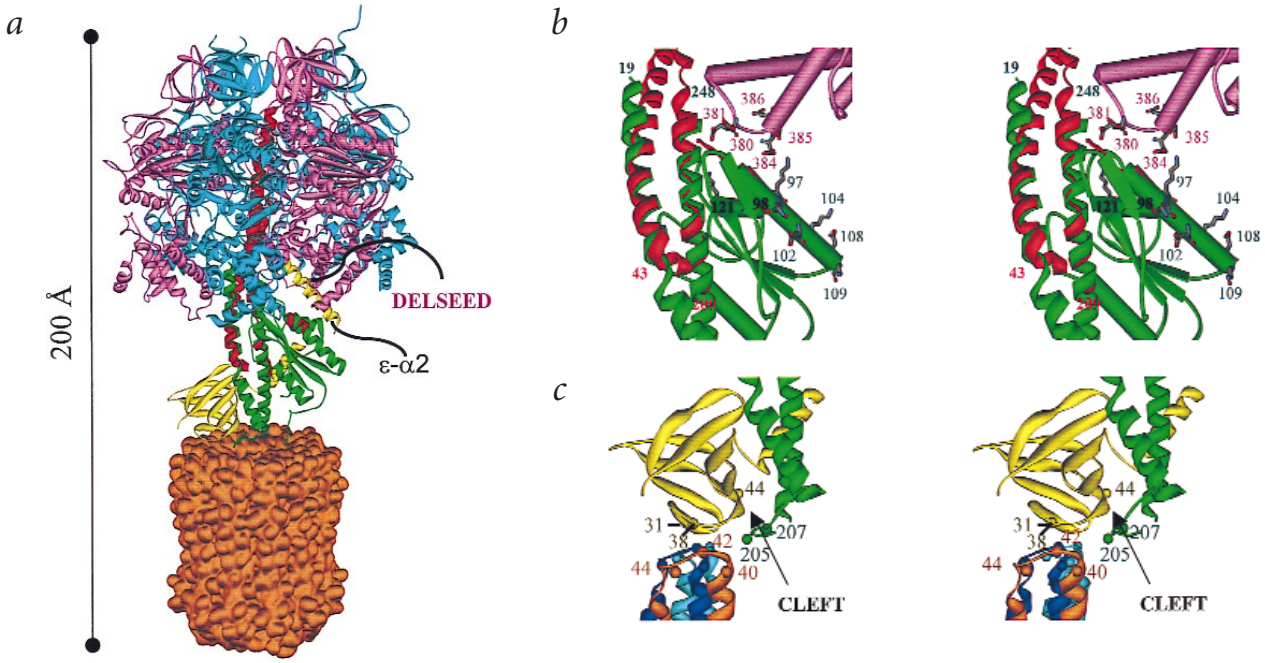

Fig. 2 Schematic representation of the composite model of ATP synthase. This model was built using a structural alignment of the common γ components of MF_1 (ref. 9) and γ′–ε and the c-subunit ring[31] was positioned based upon crosslinking studies between γ, ε and c. Structurally aligned residues include γ-subunit residues 27–41 and 209–232 in MF_1 (residues 29–43 and 224–247 in *E. coli*) and the α2 helix residues 77–90 in MF_1 (residues 87–100 in *E. coli*). The position of the β-subunit DELSEED loop that would be interacting with γ is indicated. Color scheme: α-subunits, cyan; β-subunits, pink; γ-subunit (MF_1), red; γ-subunit (*E. coli*), green; ε-subunit, yellow; c-subunit ring, orange. ***a***, The composite structure. ***b***, Close-up view of the juxtaposition of the DELSEED loop with respect to the γ-subunit. Charged residue side chains are shown and labeled. The ε-subunit has been excluded from this panel for clarity. ***c***, Close-up view of interaction between γ′–ε and the c-subunit ring. Cα positions of crosslinked residues are shown as matching colored spheres. Three c-ring subunits are shown in orange, blue and cyan and the residue numbers are color coded to match the structural components.

212–247 (γ-α6), which are twisted into a coiled coil (Fig. 1*b*). The coiled coil helices of the γ-subunit span the entire complex. Amino acid Pro 43 induces a kink in γ-α1 of ~20°, but the direction of the bend is such that close contacts between the helices are maintained along their entire lengths. The plane of the β-sandwich of ε is aligned parallel to the coiled coil, with the β-strands approximately orthogonal to the direction of the helices. The extended helices of ε entwine γ, wrapping approximately halfway around its core. The portion of the γ-subunit lying on the opposite side of the coiled coil from the ε-subunit β-sandwich is a helix-sheet-helix domain, featuring a five-stranded β-sheet wedged between two α-helices formed by residues 91–108 (γ-α3) and 150–161 (γ-α5). The first four of these strands (residues 74–80 (γ-β1), 111–117 (γ-β2), 135–138 (γ-β3) and 166–174 (γ-β4)) are in parallel conformation, while the fifth (residues 179–183, γ-β5), and shortest, runs antiparallel to the fourth. A short α-helix (residues 120–124, γ-α4) connects the second and third β-strands (Fig. 1*c*). The structure of the γ-subunit contrasts with that determined by Hausrath *et al.*[11] from 4.4 Å resolution data of the γ-subunit within the *E. coli* F_1. While γ-α1, γ-α3 and γ-α6 are similarly positioned, the remainder of the structure contains quite different secondary and tertiary structural elements, most likely reflecting difficulties in interpreting electron density at moderate resolution.

Composite structure of ATP synthase

The γ′–ε structure can be viewed in conjunction with the bovine MF_1 structure to picture the way that these components of the enzyme are likely to interact (Fig. 2). The γ-subunits from both structures were superimposed using the *ab initio* alignment option in the program LSQMAN (http://xray.bmc.uu.se/usf/lsqman_man.html). This resulted in the superposition of segments of the γ-subunit coiled coil (residues 27–41 and 209–232 in MF_1; residues 29–43 and 224–247 in *E. coli* γ′–ε) and the α2 helix (residues 77–90 in MF_1; residues 87–100 in *E. coli* γ′–ε) with an r.m.s. deviation of 1.4 Å on these 53 Cα atoms. The alignment also corresponds to the CLUSTAL X (http://www2.ebi.ac.uk/clustalw) alignment of the two sequences, which show an overall identity of 34% for the superimposed region. This composite structure shows that the pair of γ-subunit coiled helices stretches from the top of the $\alpha_3\beta_3$ hexamer to the bottom of the γ–ε complex, consistent with a recent low resolution structure of the *E. coli* F_1 (ref. 11). This feature could act as an axle, around which the γ–ε complex can rotate. The proximity of both coiled helices γ-α1 and γ-α6 to the ε-subunit would explain the results that residues ε10, ε38 and ε43 could be crosslinked to the C-terminal portion of the γ-subunit in F_1 (ref. 15), and the effects of mutations on the same face of the ε β-sandwich (S65A, E70A, T77A and D81A), which reduce the binding affinity of ε to F_1 (ref. 16). It should be noted that in the composite model the C-terminal end of helix ε-α2 clashes sterically to a small degree with the adjacent β-subunit. The alignment of the ε β-sandwich in the composite MF_1–γ′–ε structure differs markedly from a recently published model of yeast F_1F_o (ref. 17), in which the ε β-sandwich lies parallel to the surface of the membrane. Disruption of the arrangement of some of the subunits at the interface between F_o and F_1 due to the use of detergent in the preparation of the yeast enzyme might account for this discrepancy.

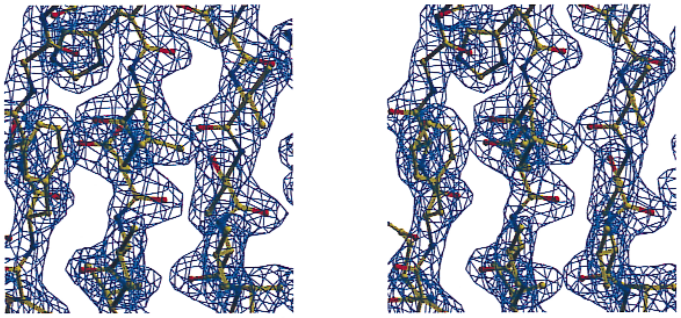

Fig. 3 Stereo view of the $2F_o$ - F_c electron density map at 2.1 Å resolution, which is contoured at 1.4 σ. A region within the β-sandwich of the ε-subunit is shown (from left to right, residues 15–18, 5–8 and 75–79). This figure was generated using O[28].

The γ′–ε structure (Fig. 1*a*,*b*) shows that the conformation of the N-terminal β-sandwich of the ε-subunit is very similar to the crystal[12] and NMR[13] structures of the isolated protein, but that the arrangement of the C-terminal helices is dramatically different. In these structures, the helices form a tight hairpin, and both interact with the β-sandwich. In contrast, the structure of γ′–ε shows the helices to be separated from one another and from the β-sandwich, and wrapped around the outside of the γ-subunit. However, the alignment of the ε-subunit helices within the F_1F_o complex is uncertain, since crosslinking, which locks the two C-terminal helices together or holds the C-terminal helix ε-α2 against the β-sandwich, has little effect on enzyme function[18]. When considered in conjunction with the structure of γ′–ε presented here, these results suggest that these helices possess considerable freedom of movement within F_1F_o. Movement of the ε helices is consistent with other observations. Crosslinking experiments showed that the C-terminal helix ε-α2 spans and interacts with the DELSEED (residues 380–386) regions of two β-subunits following ATP hydrolysis in the catalytic sites[19], but that these interactions are disrupted upon subsequent binding of ATP. Nucleotide occupancy dependent changes in ε-subunit conformation have also been observed in tryptic proteolysis experiments[20]. In the composite MF_1–γ′–ε structure (Fig. 2*a*) it is clear that the top of the β-sandwich is at least 10 Å from the DELSEED regions of the β-subunits. The C-terminal helix ε-α2 cannot simultaneously interact with two β-subunits and with either the helix ε-α1 or the β-sandwich domain, indicating that the C-terminal helical domain of the ε-subunit must undergo large movements over the catalytic cycle. Such movements may arise as the γ-subunit and β-subunit interact. It is of interest that γ–α3, which is juxtaposed directly beneath the functionally important DELSEED region, contains numerous charged residues (Fig 2*b*). In particular, several Lys residues are positioned such that they could form salt bridges with the acidic functional groups of the DELSEED sequence. Such interactions may underlie the conformational changes of the ATPase subunits during the catalytic cycle.

The γ′–ε structure provides novel insights into the importance of ε within ATP synthase. The ε-subunit is required for binding of F_1 to F_o, and inhibits ATPase activity in soluble F_1 by slowing the release of product[21]. A deletion mutant of ε in which only the first 93 residues remain partially inhibits ATPase activity and promotes binding of F_1 to F_o, while a shorter version of 80 residues retains binding function but loses inhibitory characteristics[22]. The γ′–ε structure allows this result to be understood more clearly, by showing that the helical domains of ε are separated and more mobile relative to each other than suggested by the NMR and crystal structures of the isolated subunit. The C-terminal helix ε-α2 makes close contact with the bottom of the $\alpha_3\beta_3$ hexamer and may inhibit ATPase activity by increasing the drag on rotation of γ–ε. The helix ε-α1 has much less contact with the $\alpha_3\beta_3$ hexamer, and its removal would be expected to have a greater effect on ε binding to F_1 than inhibition of enzyme activity.

Transmission of conformational changes

The structure of γ′–ε presented here sheds new light on the question of which structural elements within γ–ε play the major role of transmitting conformational changes from F_o to F_1 during catalysis. Models have been proposed[23] in which the eccentric rotation of the γ-subunit coiled coil helices alone forces the sequential conformational changes in the catalytic β-subunits predicted by the binding change mechanism. Inspection of the composite MF_1–γ′–ε structure indicates that both ε-α2 and the helix-sheet-helix domain of the γ-subunit are also likely to collide with the C-terminal domain of at least one β-subunit during each 360° rotation. The retention of enzyme activity by ε mutants lacking helix ε-α2 suggests that this domain does not greatly influence the conformations of the catalytic sites during rotation. The combined effects of the γ-subunit helix-sheet-helix domain contacting the bottom of the β-subunit C-terminal domains, and the outward force on these domains exerted by eccentric rotation of the coiled coil, are most likely responsible for altering the nucleotide binding affinities of the β-subunits as the γ–ε complex rotates. The ε-subunit β-sandwich lies on the opposite side of the γ-subunit coiled coil helices from the helix-sheet-helix domain, in contact with the membrane. The sandwich is, therefore, unlikely to play any direct role in influencing the conformations of the β-subunits during rotation, but may be important in the binding of the γ–ε complex to the c-subunit ring.

Disulfide crosslinking experiments have shown that a continuous stretch of residues (26–33) in the ε-subunit[24], along with γ-subunit residues γ-Tyr 205 and γ-Tyr 207 (refs 25,26) are in contact with the polar loop region of the c-subunit. These results are entirely consistent with the structure of the γ′–ε complex presented here. When viewed from side-on with the N- and C-terminal portions of the γ-subunit at the 'top' of the complex, these residues form part of an exposed flat surface at the bottom of the structure. A cleft is present on this surface, bounded by γ-subunit residues 203–209 on one side, and the sixth β-strand of ε (residues 41–45) on the other (Fig. 2*c*). This strand lies on the opposite face of the ε β-sandwich to the segment containing residues 26–33. It therefore seems likely that in ε E31C and γ Y205C mutants, crosslinks are formed to c-subunit Q42C residues on different, but adjacent, c-subunit polar loops. One c-subunit polar loop could probably fit within the cleft, and another would lie against the lower portion of the γ-subunit coiled coil (Fig. 2*c*). On this basis, the γ–ε complex would be expected to shield at least three adjacent c-subunit polar loops, consistent with labeling studies[27].

The structure of the γ′–ε complex presented here allows the structural information already available for the F_1 and F_o portions of ATP synthase to be connected for the first time, and suggests the mechanism by which the rotation of F_o may be coupled to F_1, resulting in ATP synthesis and release. To further advance our understanding of this enzyme, detailed structural information on F_o will be required, so that the proton path across the

Table 1 Crystallographic statistics

Data collection				
Data set	Resolution (Å)	Reflections (measured/unique)	Completeness (%; overall/outer shell)	R_{sym} (%; overall/outer shell)
λ_1 (0.9795 Å)	30.0–3.0	55,502 / 8,958	99.2 / 98.1	3.3 / 9.0
λ_1 (0.9793Å)	30.0–3.0	55,552 / 8,960	99.2 / 98.1	4.0 / 12.0
λ_1 (0.9537Å)	30.0–3.0	55,550 / 8,959	99.2 / 98.1	3.2 / 8.0
Overall MAD figure of merit	0.81			
Refinement statistics				
Resolution (Å)	50–2.1	R.m.s. deviations		
R_{sym}[1] (%)	4.8	Bond lengths (Å)	0.010	
Completeness (%)	93.5	Bond angles (°)	1.69	
R-factor[2] (overall / outer shell 2.17–2.1 Å)	20.1 / 29.1	Thermal parameters (Å^2)	1.3	
R_{free} (overall / outer shell)	26.5 / 36.1			

[1]$R_{sym} = \Sigma| I - <I>| / |<I>|$.
[2]R-factor = $\Sigma||F_o| - |F_C|| / \Sigma| F_o|$ where $|F_o|$ = observed structure factor amplitudes and $|F_c|$ = calculated structure factor amplitudes.

membrane may be more clearly defined. The nature of interactions at the interface between the c-subunit ring and the γ–ε complex must also be identified, so that conformational changes in γ–ε resulting from proton flow through F_o may be elucidated. These are among many future challenges that must be overcome to fully understand the workings of this intriguing enzyme that underpins the essential energy conversion mechanism of the cell.

Methods

Bacterial expression and purification of the γ′–ε complex. The ε-subunit, along with a fusion of glutathione-S-transferase (GST) and the central domain of the γ-subunit (γ′, residues 11–258), were expressed in *E. coli* (XL-1 Blue, Stratagene) in Luria Broth at 310 K from the same plasmid. The cells were induced using isopropyl-β-thiogalactopyranoside (IPTG) at an OD = 590 nm of 1.0 and harvested 3 h later. The GST–γ′–ε complex was purified by glutathione-agarose affinity chromatography (Sigma). Following digestion with thrombin to cleave the GST moiety from the GST fusion protein, the γ′–ε complex was purified by anion exchange (Biorad Q1 column) and gel filtration chromatography (Biorad SE1000 gel). When required, selenomethionine (SeMet) was incorporated into the protein by growing the cells in minimal medium containing SeMet (50 μg ml^{-1}) along with Lys, Thr and Iso (100 μg ml^{-1}).

Crystallization. The γ′–ε complex was crystallized from 0.5 M tartrate buffered with 0.1 M Tris-HCl at pH 8.8 (space group $C222_1$, a = 76.7 Å, b = 176.1 Å, c = 67.1 Å) by hanging drop vapor diffusion at 22 °C. Native and multiwavelength anomalous dispersion (MAD) data were collected under cryogenic conditions using the Advanced Photon Source (APS) beamline 14C. Crystals were transferred to mother liquor containing 20% (w/v) glycerol as a cryoprotectant just prior to data collection.

Structure determination and refinement. Sixteen selenium atoms were located using anomalous difference Patterson syntheses. MAD phases at 3.0 Å resolution yielded an interpretable electron density map. After model building using O[28], the structure was refined to convergence at 2.1 Å resolution using CNS[29]. PROCHECK[30] revealed no unfavorable (φ,ψ) combinations in the γ′–ε complex, with main chain and side chain structural parameters consistently better than average (overall G value 0.2). The electron density was readily interpretable for residues 1–105, 110–134 of the ε-subunit, and 18–58, 62–193, and 200–248 of the γ′-subunit. Missing loops were excluded from the model. An electron density map is included in Fig. 3.

Coordinates. The structural coordinates have been deposited in the Protein Data Bank (accession code 1FS0).

Acknowledgments
Use of the APS was supported by the US Department of Energy, Basic Energy Sciences, Office of Science. Use of the BioCARS Sector 14 was supported by the National Institutes of Health, National Center for Research Resources. This research was supported by grants from the National Health and Medical Research Foundation (M.C.J.W.), University of Western Australia Medical Research Fellowship (A.J.W.R.) and The Raine Medical Research Foundation (M.C.J.W.). Travel to the APS was funded from a grant from the Australian Nuclear Science and Technology Organization.

Correspondence should be addressed to M.C.J.W.
email: mwilce@receptor.pharm.uwa.edu.au

Received 19 June, 2000; accepted 26 September, 2000.

1. Senior, A.E. *Annu. Rev. Biophys. Biophys. Chem.* **19**, 7–41 (1990).
2. Fillingame, R.H., Jones, P.C., Jiang, W., Valiyaveetil, F.I. & Dmitriev, O.Y. *Biochim. Biophys. Acta* **1365**, 135–142 (1998)
3. Boyer, P.D. *Biochim. Biophys. Acta* **1140**, 215–250 (1993)
4. Duncan, T.M., Bulygin, V.V., Zhou, Y., Hutcheon, M.L. & Cross, R.L. *Proc. Natl. Acad. Sci. USA* **92**, 10964–10968 (1995).
5. Sabbert, D., Engelbrecht, S. & Junge, W. *Nature* **381**, 623–625 (1996).
6. Noji, H., Yasuda, R., Yoshida, M. & Kinosita, K., Jr. *Nature* **386**, 299–302 (1997).
7. Bulygin, V.V., Duncan, T.M. & Cross, R.L. *J. Biol. Chem.* **273**, 31765–31769 (1998)
8. Kato-Yamada, Y., Noji, H., Yasuda, R., Kinosita, K. and Yoshida, M. *J. Biol. Chem.* **273**, 19375–19377 (1998)
9. Abrahams, J.P., Leslie, A.G., Lutter, R. & Walker, J.E. *Nature* **370**, 621–628 (1994).
10. Bianchet, M.A., Hullihen, J., Pedersen, P.L. & Amzel, L.M. *Proc. Natl. Acad. Sci. USA* **95**, 11065–11070 (1998).
11. Hausrath, A.C., Grüber, G., Matthews, B.W. & Capaldi, R.A. *Proc. Natl. Acad. Sci.* **96**, 13697–13702 (1999).
12. Wilkens, S., Dahlquist, F.W., McIntosh, L.P., Donaldson, L.W. & Capaldi, R.A. *Nature Struct. Biol.* **2**, 961–967 (1995).
13. Uhlin, U., Cox, G.B. & Guss, J.M. *Structure* **5**, 1219–1230 (1997).
14. Dunn, S.D. *J. Biol. Chem.* **257**, 7354–7359 (1982).
15. Tang, C. & Capaldi, R.A. *J. Biol. Chem.* **271**, 3018–3024 (1996).
16. Xiong, H., Zhang, D. & Vik, S.B. *Biochemistry* **37**, 16423–16429 (1998).
17. Stock, D., Leslie, A.G. & Walker, J.E. *Science* **286**, 1700–1705 (1999).
18. Schulenberg, B. & Capaldi, R.A. *J. Biol. Chem.* **274**, 28351–28355 (1999).
19. Wilkens, S. & Capaldi, R.A. *J. Biol. Chem.* **273**, 26645–26651 (1998).
20. Mendel-Hartvig, J. & Capaldi, R.A. *Biochemistry* **30**, 1278–1284 (1991).
21. Weber, J., Dunn, S.D. & Senior, A.E. *J. Biol. Chem.* **274**, 19124–19128 (1999).
22. Kuki, M., Noumi, T., Maeda, M., Amemura, A. & Futai, M. *J. Biol. Chem.* **263**, 17437–17442 (1988).
23. Wang, H. & Oster, G. *Nature* **396**, 279–282 (1998).
24. Hermolin, J., Dmitriev, O.Y., Zhang, Y. & Fillingame, R.H. *J. Biol. Chem.* **274**, 17011–17016 (1999).
25. Watts, S. D., Tang, C. & Capaldi, R.A. *J. Biol. Chem.* **271**, 28341–28347 (1996).
26. Schulenberg, B., Aggeler, R., Murray, J. & Capaldi, R.A. *J. Biol. Chem.* **274**, 34233–34237 (1999).
27. Watts, S.D. & Capaldi, R.A. *J. Biol. Chem.* **272**, 15065–15068 (1997).
28. Jones, T.A., Zou, J-Y., Cowan, S.W. & Kjeldgaard, M. *Acta Crystallogr., A* **47**, 110–119 (1991).
29. Brunger, A.T. *et al. Acta Crystallogr. D.* **54**, 905–921 (1998).
30. Laskowski, R.J., MacArthur, M.W., Moss, D.S. & Thornton, J.M. *J. Appl. Crystallogr.* **26**, 283–290 (1993).
31. Dmitriev O.Y., Jones P.C. & Fillingame R.H. *Proc .Natl. Acad. Sci. USA* **96**, 7785–7790 (1999).